

Learning from Visual Demonstrations through Differentiable Nonlinear MPC for Personalized Autonomous Driving

Flavia Sofia Acerbo^{1,2,3}, Jan Swevers^{2,4}, Tinne Tuytelaars³ and Tong Duy Son¹

Abstract—Human-like autonomous driving controllers have the potential to enhance passenger perception of autonomous vehicles. This paper proposes DriViDOC: a model for Driving from Vision through Differentiable Optimal Control, and its application to learn personalized autonomous driving controllers from human demonstrations. DriViDOC combines the automatic inference of relevant features from camera frames with the properties of nonlinear model predictive control (NMPC), such as constraint satisfaction. Our approach leverages the differentiability of parametric NMPC, allowing for end-to-end learning of the driving model from images to control. The model is trained on an offline dataset comprising various driving styles collected on a motion-base driving simulator. During online testing, the model demonstrates successful imitation of different driving styles, and the interpreted NMPC parameters provide insights into the achievement of specific driving behaviors. Our experimental results show that DriViDOC outperforms other methods involving NMPC and neural networks, exhibiting an average improvement of 20% in imitation scores.

I. INTRODUCTION

Making automated driving functionalities more human-like can improve the perception of comfort and naturalness in autonomous vehicles (AVs), ultimately increasing their adoption rates. Driving behaviors vary among individuals, so customization of human-like AVs is needed to meet the quality expectations of all end users. While it may be complex to model or explain human behaviors using metrics and features, desired driving actions can be demonstrated by human drivers in a repeatable manner within controlled simulation environments, such as driving simulators. Therefore, the goal is to mimic the demonstrated behavior in the autonomous control systems, achieving similarity in both high-level variables (such as distances to objects) and low-level ones (like accelerations and jerks), that overall affect the perception of an AV. At the same time, it is imperative to ensure safety at all times and practical constraints, including regulations, system limits, and the efficiency of control tuning in terms of time and data, must be taken into consideration. Imitation learning (IL) algorithms offer a wide range of solutions to mimic demonstrated behaviors. However, black-box IL raises safety concerns and lacks guarantees for

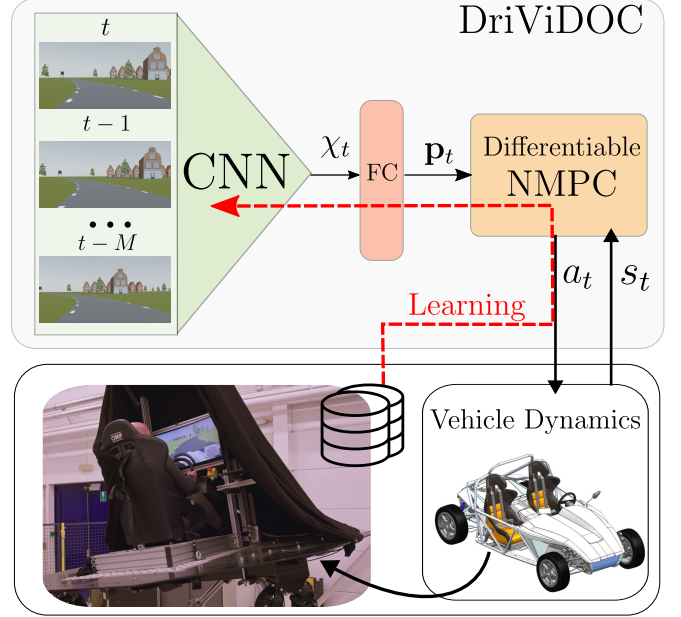


Fig. 1: DriViDOC architecture: at time t , the visually encoded information by the neural network χ_t serves to compute the parameters \mathbf{p}_t of an NMPC, which controls a high-fidelity vehicle dynamics model used for human-in-the-loop testing on a hexapod platform. The driving model is learned end-to-end from pixels to control, based on human demonstrations collected offline on the platform.

scenarios beyond training data. Nonlinear model predictive control (NMPC) integrates safety constraints and provides more explainable behavior, due to its reliance on a model, but may lack the required flexibility to imitate diverse human driving behaviors. Thus, we propose to realize customized autonomous driving with:

- 1) imitation learning from few demonstrations provided offline by a human driver,
- 2) raw sensor data as input to the driving model, so that internal representations that determine the demonstrated driving style are automatically inferred,
- 3) nonlinear MPC, to satisfy safety and system constraints and cope with multi-variate complex dynamics,
- 4) closed-loop tests with a high-fidelity dynamic car model, to be deployed on motion-base driving simulators.

To enable this, we leverage the *differentiability* of the NMPC. This allows us to compute the sensitivity of the optimal control action with respect to the NMPC parameters, which is essential to perform backpropagation through it. By doing

¹Siemens Digital Industries Software, Leuven, Belgium

²Dept. of Mechanical Engineering, KU Leuven, Belgium

³Dept. of Electrical Engineering (ESAT), KU Leuven, Belgium

⁴Flanders Make@KU Leuven, Leuven, Belgium

Corresponding author email: flavia.acerbo@siemens.com

© 2024 IEEE. Personal use of this material is permitted. Permission from IEEE must be obtained for all other uses, in any current or future media, including reprinting/republishing this material for advertising or promotional purposes, creating new collective works, for resale or redistribution to servers or lists, or reuse of any copyrighted component of this work in other works.

so, we learn how to map high-dimensional data to safe and feasible low-level control actions without disrupting the end-to-end pipeline, as shown in Fig. 1. Summarizing, the contributions of this paper are:

- 1) development of DriViDOC (Driving from Vision through Differentiable Optimal Control), an end-to-end differentiable driving model cascading a deep convolutional network with NMPC, mapping raw camera images to control actions through dynamic NMPC parameters,
- 2) behavioral cloning on an offline dataset of different human driving styles, collected on a hexapod driving simulator,
- 3) evaluation of DriViDOC performance, in closed-loop simulations, compared to other state-of-the-art methods involving both neural networks and NMPC, showing the advantages of considering the NMPC already in the training phase and the value of learning latent representations from camera images.

The paper is structured as follows: first, we discuss previous work on imitation learning for AVs, and its integration with NMPC, including our previous work in this domain; second, we describe the main components of DriViDOC; third, we provide details on the dataset, training and testing procedures, and results of the learning for different drivers; finally, we compare our method with other approaches.

II. RELATED WORK

End-to-end autonomous driving is historically mapping images to control actions. However, to obtain safer controllers and more sample efficient learning algorithms, research has moved in the direction of hierarchical architectures. In such frameworks, imitation happens on high-level driving data, e.g. end-goals, waypoints. Often, an MPC serves as the low-level tracker to enhance safety, leveraging its capability to satisfy constraints. However, the design of the tracking control influences the passenger perception, which becomes of paramount importance when moving to human-in-the-loop tests with subjective feedback. Recently, there have been works where the high-level planner takes into account the effect of the low-level tracker, e.g. [1]. However, these works do not: 1) exploit the differentiability of MPC, making it a part of the learnable policy, 2) operate on raw image input, which in turn can contain useful features that would be challenging for engineers to anticipate.

Another research direction to add safety to end-to-end controllers is the use of MPC as a *predictive safety filter* [2], i.e. as a component that, given a desired control action, checks whether a plan to a safe terminal set exists by applying that control action, and corrects it if necessary. However, even if the corrected actions are considered safe, the imitation performance may be compromised. In [2], [3], the authors compensate for that by using on-policy learning, with an NMPC as interactive expert. Nevertheless, in our scenario humans are the expert driver, and it is not possible to have them acting as interactive experts.

Finally, the use of differentiable NMPC as a policy substitute for neural network structures is an active area of research. In [4], NMPC static parameters in the objective function and model are learned through IL for reinforcement learning benchmarks. However, differentiable NMPC and neural networks can also complement one another. For example, in [5], the authors show a similar architecture to ours for robotic navigation in human-occupied spaces, utilizing a differentiable NMPC with a learned dynamic cost based on a latent embedding of the current occupancy map. Our recent research explored the application of NMPC and IL to achieve human-like autonomous driving. We demonstrated optimal results in terms of imitation, safety, and comfort by dynamic parametrization of the NMPC from preceding network layers [6]. However, our previous work only focused on fully-connected models with predetermined features as inputs, and we compared our method against others that employed either NMPC with static parameters or neural network architectures. In contrast, DriViDOC allows for direct learning from raw images, and in this study, we compare it to methodologies that combine both NMPC and neural networks.

III. DriViDOC: DRIVING FROM VISION THROUGH DIFFERENTIABLE OPTIMAL CONTROL

In our approach, an NMPC incorporates various parameters in its objective function, wherein their relative values directly influence the control style (e.g. tradeoff between desired speed and applied acceleration). Traditionally, these parameters are manually set, but with the differentiability of the NMPC, we can automatically learn them. To capture the intricacies of multiple human driving behaviors, DriViDOC uses dynamic parameterization, i.e. instead of assuming a fixed set of NMPC parameters, different combinations are utilized based on the driving context. This driving context is embedded from front camera images by a convolutional neural network (CNN), which is trained to predict the NMPC parameters that best replicate the behavior of a given human driver. In the following we introduce the four key components of DriViDOC: the NMPC formulation, the calculation of its derivatives with respect to parameters, its connection to the neural network layers, and the imitation learning algorithm.

Let us consider a generic *parametric* NMPC, which at time t computes the optimal action $a_t \in \mathbb{R}^{n_u}$ for the current state $s_t \in \mathbb{R}^{n_x}$. It does so by optimizing for future states $\mathbf{x} \in \mathbb{R}^{Nn_x}$ and controls $\mathbf{u} \in \mathbb{R}^{(N-1)n_u}$. According to the receding horizon principle, the optimal action to be applied to the system is $a_t = u_0$. The scalar objective function $l : \mathbb{R}^{Nn_x} \times \mathbb{R}^{(N-1)n_u} \times \mathbb{R}^{n_p} \rightarrow \mathbb{R}$, composed of a stage cost l_k and an optional terminal cost l_N , depends on a set of parameters $\mathbf{p} \in \mathbb{R}^{n_p}$. This corresponds to solving the following nonlinear

program (NLP):

$$\begin{aligned} \min_{\mathbf{x}, \mathbf{u}} \quad & \sum_{k=0}^{N-1} l_k(x_k, u_k, \mathbf{p}) + l_N(x_N, \mathbf{p}) \\ \text{s. t.} \quad & x_0 = s_t, \\ & x_{k+1} = f(x_k, u_k), \quad \forall k = 0, \dots, N-1, \\ & h(x_k, u_k) \leq 0, \quad \forall k = 0, \dots, N-1. \end{aligned} \quad (1)$$

We assume that the model f and the inequality constraints h do not depend on \mathbf{p} ; in other words, vehicle dynamics, as well as state and actuator constraints, are known and fixed. Additionally, we assume that the current state s_t can be measured or estimated using other sensors. We adopt a *multiple shooting* solution strategy for (1). In this approach, the optimization variables are the both discretized states \mathbf{x} and controls \mathbf{u} . These variables are computed by integrating f , which represents a discretized version of the model dynamics characterized by ordinary differential equations, across a prediction horizon consisting of N equally spaced steps. The solution to the NLP can be obtained using any numerical solver of choice.

To learn the parameters \mathbf{p} through gradient-based optimization, we need to consider a differentiable version of the NMPC. In this paragraph, we discuss how to compute the derivatives of a solution of the NLP with respect to its parameters. The Lagrangian of Eq. (1) is:

$$\begin{aligned} \mathcal{L}(\mathbf{x}, \mathbf{u}, \mu, \lambda, \mathbf{p}) = & \sum_{k=0}^{N-1} l_k(x_k, u_k, \mathbf{p}) + l_N(x_N, \mathbf{p}) \\ & + \mu^T h(\mathbf{x}, \mathbf{u}) + \lambda_0^T (x_0 - s_t) \\ & + \sum_{k=0}^{N-1} \lambda_{k+1}^T [f(x_k, u_k) - x_{k+1}], \end{aligned} \quad (2)$$

where $\mu \in \mathbb{R}^N, \lambda \in \mathbb{R}^N$ are the multipliers associated to the dual problem. Now let us assume that l, f and h are twice-differentiable and that $z^* = [\mathbf{x}^*, \mathbf{u}^*]$ is a local minimum of (1). If the problem is quasi-regular, i.e. if the linear independence constraint qualification (LICQ) condition holds at z^* , then we can find μ^* and λ^* that satisfy the following Karush-Kuhn-Tucker (KKT) conditions:

$$\nabla_z \mathcal{L}(\mathbf{x}^*, \mathbf{u}^*, \mu^*, \lambda^*, \mathbf{p}) = 0, \quad (3)$$

$$x_0^* = s_t, \quad (4)$$

$$x_{k+1}^* - f(x_k^*, u_k^*) = 0, \forall k = 0, \dots, N-1, \quad (5)$$

$$h(x_k^*, u_k^*) \leq 0, \forall k = 0, \dots, N-1, \quad (6)$$

$$\mu_k^* \geq 0, \forall k = 0, \dots, N-1, \quad (7)$$

$$\mu_k^* h(x_k^*, u_k^*) = 0, \forall k = 0, \dots, N-1. \quad (8)$$

From [7], we know that if, in addition to LICQ, also second order sufficient condition (SOSC) hold for z^* , i.e. $\nabla_{zz}^2 \mathcal{L}(\mathbf{x}^*, \mathbf{u}^*, \mu^*, \lambda^*, \mathbf{p})$ is positive definite over the directions defined by the critical cone, and $\mu_k^* > 0$ when $h(x_k^*, u_k^*) = 0$, then z^* is a *local isolated* minimizing point of (1) and that μ^* and λ^* are unique. In this case, we can write the KKT conditions as an implicit function $F(z, \mathbf{p}) \iff z = G(\mathbf{p})$,

where the matrix F is guaranteed to be non-singular. The derivatives are given by the *implicit function theorem* as:

$$\frac{\partial G_{\mathbf{p}}}{\partial \mathbf{p}} = - \left(\frac{\partial F}{\partial z} \right)^{-1} \frac{\partial F}{\partial \mathbf{p}}. \quad (9)$$

The complete Jacobian of (9) may be prohibitively expensive to compute, but it is possible to compute the *adjoint sensitivities*, that are the vector-times-Jacobian product, given any vector \bar{z} , as in the following:

$$\bar{\mathbf{p}} = \left[\frac{\partial G_{\mathbf{p}}}{\partial \mathbf{p}} \right]^T \bar{z}. \quad (10)$$

In backpropagation, \bar{z} happens to be the gradient of a scalar loss function L , e.g. BC imitation loss, with respect to z . Then, by the chain rule, (10) would be the gradient of L with respect to the NMPC parameters \mathbf{p} . The computation of (10) can be done in CasADi [8] at the cost of a linear system solve and a reverse mode algorithmic differentiation pass, as shown in [9]. Differently from [4], the gradient computation is decoupled from the solution, so problem (1) can be solved with any method as long as it returns a primal-dual solution.

As previously mentioned, in DriViDOC the parameters \mathbf{p} of the NMPC are not constant, but varying in time and depending on visual data. More specifically, a deep convolutional neural network (CNN) takes a series of frames $\{I_t, I_{t-1}, \dots, I_{t-M}\}$ and processes them by a sequence of convolutional layers. These layers act as a visual encoder and the resulting latent representation χ_t is given to a sequence of fully-connected (FC) layers with n_p heads, which predict the parameters $\mathbf{p}(\chi(I_t, I_{t-1}, \dots, I_{t-M}))$ for the NMPC. Note that the SOSC condition for NMPC differentiability depend on the value of \mathbf{p}_t too.

Finally, the model can be learned on a dataset of $\{I_t, s_t, a_t\}$ tuples, backpropagating the loss from a_t until the CNN tunable parameters. The loss depends on the chosen IL algorithm and many are suitable for this purpose. However, in our setting it should be taken into account that a human interactive expert is unrealizable and that online interactions with the combined sensor and vehicle dynamics high-fidelity simulation environment are costly. Therefore, we employ *behavioral cloning* (BC), which reduces the IL problem to offline supervised learning. BC is susceptible to the well-known problem of *covariate shift*. However, this challenge can be mitigated through techniques such as data augmentation and the use of modified loss functions or layers with models and constraints [10], as is the case for the NMPC layer, which provides a form of strong inductive bias for IL.

IV. IMITATION LEARNING ON A DIVERSE HUMAN DRIVING DATASET

In this section we present the application of DriViDOC to the specific context of personalized autonomous driving, on a diverse driving dataset collected on the hexapod platform shown in Fig. 1. First, we present more details about the dataset; second, we detail the architecture of the CNN and the NMPC formulation; third, we outline the training procedure; fourth, we present qualitative results from the closed-loop

tests and finally we propose metrics to quantitatively measure the human-likeness of the learned models.

A. Dataset

The dataset was collected on a 6-degree of freedom Stewart platform (MOOG MB-EP-6DOF/24/2800kg) [11]. The scenario, designed in Simcenter Prescan [12], consists of a one-lane road 4.5m wide, delimited with a dashed line at both sides and with randomly placed road furniture. The road presents 8 clothoidal curves, each made up of a sequence of: straight line, linearly increasing curvature, constant curvature and linearly decreasing curvature. Following the convention of positive curvature for left curves and negative for right one, the radii of curvature are the following, in meters: [90, -90, 100, -100, 110, -110, 120, -120]. The vehicle is modelled in Simcenter Amesim [13] as a 15 DoF vehicle, based on real experimental data of a Siemens Simrod car [14]. The model takes into account chassis, tire, powertrain and brake dynamics, steering wheel torque feedback, and aerodynamic effects. 11 drivers participated in the study, and were asked to perform 2 or 3 trial laps before recording. Following the trial, each participant drove for 5 laps, corresponding to a duration of approximately 15 minutes. The drivers were asked to stay in the lane and keep a speed between 60 and 80 km/h. The drivers could monitor their current speed via a speedometer present on the screen.

The resulting dataset consists of 113,768 samples, with a frame rate of 10Hz. Each sample is composed of an image I_t and the set of state variables computed from the vehicle model, encompassing linear and angular positions, velocities and accelerations. The data shows diverse behaviors between drivers around many aspects. In Figure 2a, we provide an illustrative example of the distribution of longitudinal speed for four sample drivers across the recorded laps, exhibiting variations in both mean value and variance. Furthermore, in Figure 2b, we present a map of the experimental track and depict the positions within the lanes for the same four sample drivers as they approach the first curve. This visualization highlights the different preferred approaches, including maintaining the center, staying on the inner side, or anticipating the curve by positioning on the outside and entering at different timings.

B. NMPC and CNN Design

The NMPC is designed to perform path following based on a dynamic single-track vehicle model, as described in [15], in a Frenet coordinate system with respect to the road centerline, as defined in [6]. The control actions \mathbf{u} are the steering wheel angle rate $\dot{\delta}$ and the normalized throttle t_r . The states are the linear velocities v_x, v_y , in a car body frame with x pointing forward, the yaw angle rate $\dot{\psi}$, the Frenet coordinates σ, d, θ , and the steering wheel angle δ . The Frenet coordinates evolve according to the road curvature $\kappa(\sigma)$, that we assume as known. The dynamic equations are discretized and integrated over the prediction horizon with Runge Kutta 4. The horizon is set at 1.5 seconds, with a

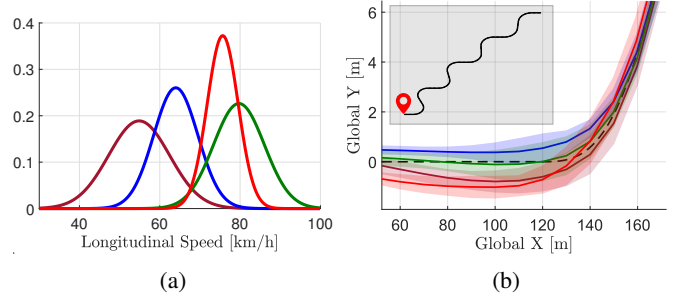


Fig. 2: Illustrations of four different driving styles present in the dataset. In (a): the Gaussian probability distributions fitted to v_x for four different drivers. In (b): position with respect to the centerline (dashed line) for the same drivers while entering the first curve of the track, in global cartesian coordinates. Inside the plot, a minimized map of the track is included.

sampling rate of 0.1 seconds, resulting in $N = 15$. Following the notation of (1), we also define the objective function:

$$l_k = W_d(d_k - \bar{d})^2 + W_v(v_{xk} - \bar{v}_x)^2 + W_{\delta}(\dot{\delta}_k)^2 + W_{t_r}(t_{rk})^2 + \gamma(d_k^2 + \theta_k^2 + \delta_k^2 + \dot{\delta}_k^2 + t_{rk}^2), \quad (11)$$

where $\mathbf{p} = [W_d, \bar{d}, W_v, \bar{v}_x, W_{\delta}, W_{t_r}]^T$ and the last term with $\gamma \ll 1$ is added for regularization and to ensure SOSC. No terminal cost l_N is defined. In (11), before the variables in are squared and summed, they are all scaled to be between $[-1, 1]$. The inequality constraints consist of a lane boundary constraint $-\frac{w}{2} \leq d_k \leq \frac{w}{2}$, a speed limit constraint $v_{min} \leq v_{xk} \leq v_{max}$, and the rest constraining all other states and control inputs to a feasible set, according to system specifications. The solution of the NLP is computed through IPOPT.

On the other hand, the CNN architecture is inspired by [16], with some modifications on the input channels and on the final decision layers. This choice is taken prioritizing a lightweight structure, needed for future real-time deployment of the model. More specifically, let I_t denote the t -th frame of a front camera stream. Past information is included by concatenating the last $M = 3$ frames on the channels as input to our CNN, so that it accepts $3(M + 1)$ channels. Then, the concatenated frames are processed by five 2×2 convolutional layers of 24, 36, 48, 64, 64 output channels each. The resulting 1152 element latent variable χ_t is fed to a two-layer fully-connected network with 100 and 50 neurons. Finally, $n_p = 6$ one-layer heads predict the parameters \mathbf{p}_t . The heads associated to the objective function weights have a ReLU activation function on the output, to guarantee the SOSC for NMPC differentiability, while the ones associated with offsets have a \tanh , to map the offsets between limits that are compatible with the constraints. We refer to the learnable weights and biases of the CNN + FC network as $\Theta = \{W_{k=1, \dots, 5}^{(i)}, b_{k=1, \dots, 5}^{(i)}, W_{fc}^{(i,j)}, b_{fc}^{(j)}\}$.

C. Open-Loop Training

The human demonstrations are composed by tuples of images, states and actions, denoted as $\{I_t^h, s_t^h, a_t^h\}$. Firstly,

image data is augmented via random perturbations of certain vehicle states, as this is shown to reduce the effect of covariate shift for behavioral cloning. For each sample, we add a perturbation to d , θ , the car altitude, and its roll and pitch angles, and we obtain a new camera frame from the simulation environment. These perturbations are sampled from Gaussian distributions centered around 0 and with standard deviations 0.20 m, 0.01 rad, 0.10 m and 0.01 rad respectively. The control actions are assumed to remain unchanged for such small perturbations. Secondly, data is partitioned and processed. The unperturbed data is split such that the samples from the curves with 110 m and -110 m radius of curvature are kept for testing and validation. The original camera frames have a resolution of 256x512 pixels. They are first cropped to 150x512, to remove big empty sky areas, then resized to 64x200 and finally normalized. The data is then balanced by downsampling straight driving samples and upsampling curved driving ones. The actions a_t^h are scaled between 0 and 1.

Finally, the driving model is trained with behavioral cloning, on a training dataset of D_{train} size, by solving the following supervised learning problem,

$$\Theta^* = \arg \min_{\Theta} \sum_{t=1}^{D_{train}} \|a_t^h - a_t(I_t^h, s_t^h)\|_2^2, \quad (12)$$

where a_t^h is sampled from the demonstrations dataset, whereas a_t represents the action computed by DriViDOC based on $\{I_t^h, s_t^h\}$, which are also sampled from the dataset together with a_t^h . Problem (12) is solved using the Adam Optimizer with an initial learning rate of 10^{-4} . The training is performed in three phases. To start, the CNN is trained separately for 100 epochs on all samples, coming from all drivers, to predict δ and v_x from camera frames. The optimal validation loss model is subsequently fine-tuned individually for each driver, utilizing 25 epochs of data specific to that driver. Then, the FC heads are modified and the NMPC is added as last layer of the driving model. CNN and NMPC together are finetuned for 25 epochs to predict $\hat{\delta}$ and t_r from camera frames and states. We train with a batch size of 10 on an NVIDIA GeForce RTX 3060 GPU (for CNN tensors) and on a Ryzen ThreadRipper 3995WX Pro (for NMPC tensors). The pretraining of the CNN on all drivers takes approximately 33 hours, while the finetuning on one driver takes about 1 hour for the CNN alone and 40 hours for both the CNN and NMPC together.

D. Closed-Loop Testing

The learned driving models are tested in closed-loop simulations, with the same high-fidelity car model and scenario used for data collection on the hexapod platform. In the following section, we present the results related to these simulations.

1) State Simulations: The considered states for the evaluation are v_x , d , a_x and a_y . In Fig. 3, we show how these cues differ for two driving models, and how they qualitatively match the corresponding demonstrated driving style. To model the mean driving style and its variance

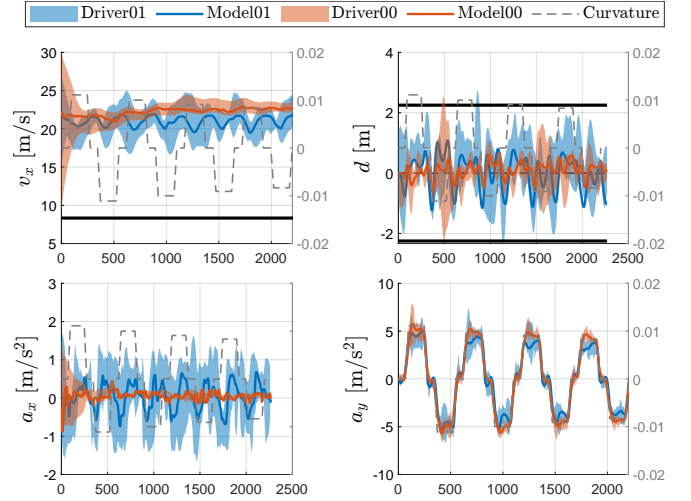


Fig. 3: Relevant states from closed-loop simulations of two DriViDOC models, compared with the corresponding driver distribution. On the right axis, we indicate the curvature with a dashed line. In the d plot, the lane boundaries are shown as horizontal solid lines.

across the repeated laps, we do the following: given the collected states for one driver, we fit Gaussian distributions for each of them in every track point (with 1m tolerance) such that each state s^h in a specific track point σ is seen as $s^h(\sigma) \sim \mathcal{N}_s(\mu_s(\sigma), SD_s(\sigma))$. In Fig. 3 we plot $SD_s(\sigma), \forall \sigma = 0, \dots, L^{track}$. Driver00 exhibits constant speed behavior, reflected in the driving model learned from this data (Model00). Conversely, Driver01 displays oscillating speed patterns along curves, characterized by deceleration from the start to the mid-point and acceleration thereafter. Model01, trained on this data, captures both the speed oscillations and longitudinal acceleration trends resulting from throttle adjustments.

2) NMPC Parameters: Having a finite set of NMPC parameters increases the interpretability of DriViDOC since the difference in driving models can be attributed to the dynamic variations in the parameters of the NMPC objective function, shown in Fig. 4. From that, we discover that the same driving model exhibits a different behavior in left and right curves, which is not evident in the state simulations. In right curves, the oscillating speed of Model01 is attributed to a decreasing and increasing behavior of W_v and W_{t_r} . In left curves, Model01 exhibits instead a constant lower W_v and null W_{t_r} . As a result, the vehicle decelerates until the longitudinal error ($|v_x - \bar{v}_x|_2^2$) becomes sufficiently large to trigger the control to accelerate again. Model00 shows instead a constant W_v , resulting in the vehicle maintaining a constant speed. Model00 shows also a preview behavior, anticipating the curve ahead when on the straight driving part, as it can be seen from the peaks of W_d when curvature is zero. This aims at positioning the vehicle ahead of the curve and hence reducing d variations when entering. From this analysis we note that the offsets are not meaningful setpoints per se, but that, combined with the weights, constitute a good parameter set for the NMPC to mimic the driving actions.

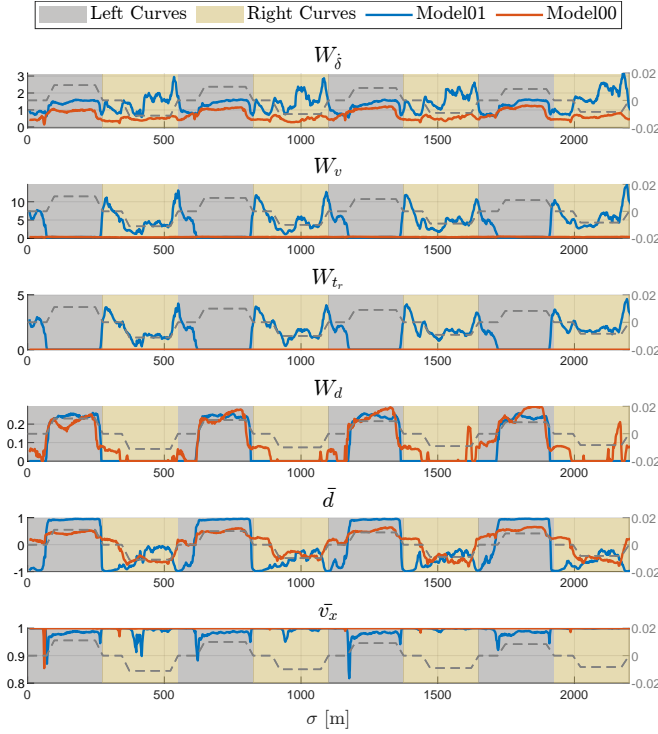


Fig. 4: On the left axis of each plot, parameters $\mathbf{p}(t)$ values from closed-loop simulations of DriViDOC models trained for 2 different drivers. The offsets \bar{d} and \bar{v}_x are normalized between -1 and 1. On the right axis, we indicate the curvature with a dashed line.

3) *Human-Likeness*: To quantify the performance of the driving models, we consider the demonstrations as a series of Gaussians as described in IV-D.1, and we compute for each relevant state s the following metrics: • Absolute Error (AE) = $|s(\sigma) - \mu_s(\sigma)|, \forall \sigma = 0, \dots, L^{track}$, • Z-score = $|s(\sigma) - \mu_s(\sigma)| / SD_s(\sigma), \forall \sigma = 0, \dots, L^{track}$, to take into account also the variance present in the demonstrations. Values that are too far from the driver distribution show a Z-score > 3 . We provide mean and standard deviation for both metrics and all drivers in Table I. On average, the errors are according to expectations, with some exceptions, due to shortcomings in the NMPC control actions. Model02 exhibits d values that deviate significantly from the demonstration distribution, primarily attributed to some rapid full throttle releases by the driver. Model03 shows a similar discrepancy on both d and a_x that can be traced back to an even more consistent use of full throttle release by the driver, resembling a discrete behavior and with zero standard deviation. Additionally, Model04 shows a_x values slightly distant from the distribution, attributed to frequent use of the brake by the driver. In contrast, the NMPC, which inherently provides a more continuous control, consistently avoids fully releasing the throttle and does not control the brake. Consequently, it maintains a speed slightly higher than the mean. This leads to the learned steering action failing to accurately position the vehicle within the lane and to the simulated longitudinal acceleration diverging from the demonstrations during hard

deceleration peaks. However, in this way, the NMPC avoids providing uncomfortable longitudinal acceleration and jerk to the passenger.

V. BENCHMARKING

In this section, we discuss experimental results of the benchmarking of DriViDOC against other baseline approaches involving neural networks and NMPC.

A. Baselines Description

1) *NMPC Tracker for a CNN Planner (TRACK)*: In this baseline, the CNN predicts \bar{d} and \bar{v}_x values. These predictions are learned in a manner such that, for each time t , the CNN maps the input frames sequence $(I_t, I_{t-1}, \dots, I_{t-M}), M = 3$ to the corresponding output vector $[d_{t+T_f}, v_{x(t+T_f)}]^T$, where T_f represents the NMPC prediction horizon (set to 1.5 seconds, corresponding to $N = 15$). These predicted values then serve as setpoints in the NMPC's objective function as follows:

$$\min_{\mathbf{x}, \mathbf{u}} \sum_{k=0}^{N-1} (d_k - \bar{d})^2 + (v_{xk} - \bar{v}_x)^2 + \gamma(\delta_k^2 + \theta_k^2 + d_k^2 + t_{rk}^2). \quad (13)$$

The CNN for these models is finetuned on data coming from the corresponding driver for 50 epochs, starting from the model trained on all drivers predicting speed and steering angle.

2) *NMPC as Safety Filter for the CNN Controller (SF)*: This method is adapted from [2]. In this approach, the CNN predicts steering angle and throttle as $a_{CNN} = [\delta, t_r]^T$. These actions are subsequently input into an NMPC to assess whether a trajectory to a terminal safe set of choice can be planned once they are applied. If not, the NMPC calculates the closest control action to ensure the feasibility of planning a trajectory to the safe set. Specifically, the NMPC is formulated as follows:

$$\min_{\mathbf{x}, \mathbf{u}} \|u_0 - a_{CNN}\|_2^2 + \gamma \sum_{k=0}^{N-1} (\delta_k^2 + \theta_k^2 + d_k^2 + t_{rk}^2) \quad (14)$$

s. t. $d_N = \theta_N = 0$.

The terminal safe set we consider is when the vehicle is fully aligned with the road. The CNN for these models is finetuned as in the TRACK baseline.

3) *Differentiable NMPC without Images (NOIMG)*: For this baseline, we aim to assess the impact of learning directly from raw representation, as opposed to using predefined features, which was demonstrated in [6]. To achieve this, we eliminate the convolutional layers. The handcrafted features, fed directly into the FC layers, are the following: $\chi_t = [v_{xt}, d_t, \theta_t, \kappa(\sigma_t), \kappa(\sigma_t + 5), \kappa(\sigma_t + 10), \dots, \kappa(\sigma + 30)]^T$, i.e. a subset of the current state and samples of the road curvature, spanning from the current track point σ_t to 30 meters ahead ($\sigma_t + 30$). The NMPC remains invariant with respect to DriViDOC. The model is trained separately for each individual driver using 25 epochs and starting from scratch. The training takes approximately 20 hours, which is less than DriViDOC, owing to the reduced size of the network and the absence of data augmentation.

TABLE I: Performance of DriViDOC for each driver, averaged across the track length. Less optimal results (Z-score > 2) are highlighted with a red colour.

	d		v_x		a_x		a_y	
	AE [m]	Z-score	AE [m/s]	Z-score	AE [m/s ²]	Z-score	AE [m/s ²]	Z-score
Model00	0.18 \pm 0.14	0.84 \pm 0.79	0.36 \pm 0.29	0.63 \pm 0.37	0.08 \pm 0.11	1.68 \pm 1.65	0.20 \pm 0.17	0.65 \pm 0.55
Model01	0.43 \pm 0.32	1.16 \pm 1.07	0.49 \pm 0.38	0.52 \pm 0.39	0.22 \pm 0.18	0.73 \pm 0.83	0.37 \pm 0.29	0.84 \pm 0.73
Model02	0.51 \pm 0.32	3.39 \pm 2.21	1.69 \pm 0.86	0.83 \pm 0.46	0.16 \pm 0.14	0.65 \pm 0.63	0.53 \pm 0.40	1.36 \pm 1.22
Model03	0.61 \pm 0.37	2.51 \pm 2.38	1.37 \pm 0.69	1.50 \pm 1.55	0.25 \pm 0.25	2.46 \pm 4.42	0.56 \pm 0.31	1.35 \pm 0.84
Model04	0.42 \pm 0.32	1.66 \pm 1.32	1.21 \pm 0.77	1.29 \pm 0.88	0.51 \pm 0.47	2.01 \pm 2.00	0.46 \pm 0.33	1.21 \pm 0.86
Model05	0.35 \pm 0.26	2.00 \pm 1.87	0.88 \pm 0.74	0.69 \pm 0.43	0.29 \pm 0.24	0.85 \pm 0.79	0.29 \pm 0.21	1.30 \pm 1.39
Model06	0.44 \pm 0.32	1.34 \pm 1.27	1.40 \pm 1.18	0.81 \pm 0.87	0.23 \pm 0.15	0.98 \pm 0.85	0.43 \pm 0.32	1.04 \pm 0.93
Model07	0.27 \pm 0.19	1.09 \pm 0.93	0.62 \pm 0.52	0.45 \pm 0.42	0.22 \pm 0.20	0.96 \pm 1.04	0.29 \pm 0.24	0.77 \pm 0.77
Model08	0.41 \pm 0.26	0.94 \pm 0.61	1.00 \pm 0.71	0.98 \pm 0.75	0.19 \pm 0.17	0.83 \pm 0.87	0.41 \pm 0.34	0.92 \pm 0.86
Model09	0.41 \pm 0.27	1.42 \pm 1.32	0.53 \pm 0.51	0.99 \pm 1.36	0.13 \pm 0.12	1.03 \pm 0.95	0.31 \pm 0.29	1.00 \pm 1.10
Model10	0.17 \pm 0.12	0.98 \pm 0.86	1.42 \pm 0.87	1.18 \pm 1.12	0.25 \pm 0.23	0.82 \pm 0.78	0.41 \pm 0.30	0.96 \pm 0.82

TABLE II: Benchmarking studies. We report performance in terms of Mean Absolute Error (MAE) and Mean Z-score (MZ) over the track. Results are averaged over all drivers, except for the NOIMG baseline for which drivers 00,03,10 and 11 have been excluded (see text). Best results are highlighted in bold.

		TRACK	SF	NOIMG	DriViDOC (Ours)
d	MAE	0.38 \pm 0.15	0.59 \pm 0.15	0.29 \pm 0.12	0.38 \pm 0.13
	MZ	1.49 \pm 0.53	2.51 \pm 0.83	1.40 \pm 0.73	1.58 \pm 0.78
v_x	MAE	1.30 \pm 0.47	2.62 \pm 2.09	2.53 \pm 0.98	1.00 \pm 0.45
	MZ	1.25 \pm 0.43	2.36 \pm 1.93	1.81 \pm 0.28	0.90 \pm 0.33
a_x	MAE	0.45 \pm 0.15	0.25 \pm 0.12	0.36 \pm 0.12	0.23 \pm 0.11
	MZ	2.72 \pm 1.17	1.20 \pm 0.74	2.05 \pm 1.53	1.18 \pm 0.59
a_y	MAE	0.50 \pm 0.17	0.67 \pm 0.39	0.65 \pm 0.19	0.39 \pm 0.11
	MZ	1.35 \pm 0.38	1.60 \pm 0.79	1.51 \pm 0.24	1.04 \pm 0.24

B. Results

The benchmarking results are summarized in Table II. For each baseline approach, we report the mean absolute error (MAE) and the mean Z-score (MZ) over the track, with mean and standard deviation for all drivers. On average, DriViDOC shows better performance on all metrics, with an average 20% relative improvement. In the following, we discuss the results for each baseline approach.

1) *TRACK*: TRACK exhibits most of its problems in the longitudinal behavior, while having better match with the driver distribution on d , with respect to DriViDOC. Since TRACK does not learn the low level control actions, the NMPC provides an unnatural behavior on the throttle. This reflects on a_x significantly far from the demonstrations, with a relative increase of 95% in MAE compared to DriViDOC. Moreover, for v_x , the model sometimes tends to provide constant references, even though the trend is not. This can be attributed to the network predicting a setpoint only 1.5 seconds ahead. In situations where changes of v_x are not significantly fast, the future state may be very close to the current one. As a result, when v_{xt} is already within the distribution, the CNN predicts $\bar{v} \approx v_{xt}$. These phenomena can be both seen in Fig. 5. Conversely, DriViDOC is less affected by a short prediction horizon, as the CNN adapts the parameters accordingly by taking into account the NMPC already in the training phase.

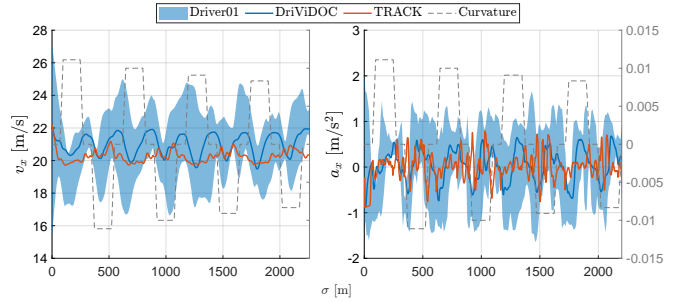
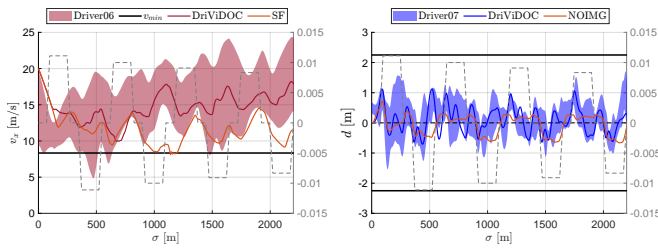


Fig. 5: DriViDOC vs TRACK baseline for Driver01 (v_x and a_x).

2) *SF*: The results with SF exhibit a clear trend toward worse imitation scores for d and v_x , with a relative increase in MAE of 54% and 162%, respectively, compared to DriViDOC. Nonetheless, some small improvements relative to DriViDOC are noticeable, particularly for a_x in 04 and 05 (drivers with throttle release and braking), as well as for 00 and 09 (drivers with quasi-constant throttle), with a mean relative reduction of 25% in MAE with respect to DriViDOC. This occurs because, during training, the NMPC does not dictate the shape of the control actions and the CNN alone finds it easier to generate such actions. On average, however, SF appears more susceptible to the covariate shift problem, tending to deviate from the driver speed distribution. It is only when the vehicle approaches a state that will lead to constraint violation that the safety filter intervenes, correcting to the closest safe control actions. However, given that the vehicle already moves beyond the training distribution, errors accumulate, and the safety filter takes over more often. Consequently, SF frequently remains close to the constraint boundary without reverting to the distribution. In DriViDOC, instead, the NMPC intrinsically tends to keep the model in the driver distribution. We give an illustrative example of the difference between the two behaviors for v_x in Fig. 6a.

3) *NOIMG*: NOIMG exhibit inconsistent behavior across drivers. Specifically, for models 00, 01, 08, and 09, the BC training loss still does not converge after 25 epochs. This corresponds to an unacceptable closed-loop behavior, characterized by an immediate deceleration followed by a constant speed at the minimum value. We argue that models experiencing training convergence issues are those corre-



(a) DriViDOC vs SF baseline for Driver06 (v_x). (b) DriViDOC vs NOIMG baseline for Driver07 (d).

Fig. 6

sponding to drivers with higher average speeds. For an easier comparison with DriViDOC and the other baselines, the NOIMG models exhibiting this behavior have been excluded from the average metrics calculation. However, even for the remaining models, there is a decrease in imitation scores, with the exception of d . In many cases, NOIMG struggles to match the changing dynamics of certain states, and provides instead a more average and repetitive behavior, as shown in Figure 6b. This suggests that, even though differentiable NMPC is central in our approach, also learning from raw images is essential to provide more flexibility when dealing with unknown or difficult-to-model features that determine a driving style.

VI. CONCLUSIONS

We presented DriViDOC: a model for Driving from Vision through Differentiable Optimal Control. This model integrates CNN and differentiable NMPC, creating an end-to-end driving model capable of learning the mapping from images to controls. The controls, derived from NMPC, are optimized using a parametric objective function, with dynamic parameters coming from the CNN. Trained on an offline dataset with BC, DriViDOC can successfully imitate different human driving styles, while taking into account lane boundaries, speed and actuators constraints. Moreover, the parameters offer precious insights on how the driving styles are realized. The model shows improvements with respect to baseline approaches including NMPC and CNN. These improvements stem both from incorporating images as inputs and from training with the differentiable NMPC. Current limitations include the lack of other dynamic agents in the collected scenarios, which would need to be included in the NMPC constraints. Future work will involve the real-time deployment of the driving model and human-in-the-loop validation.

APPENDIX

For transparency, we provide supplementary material at the following link: [https://github.com/meco-group/DriViDOC/blob/main/](https://github.com/meco-group/DriViDOC/blob/main/supplementary_material_drividoc.pdf)

supplementary_material_drividoc.pdf. There, we display the closed-loop state simulations for the other drivers, as it is shown for 00 and 01 in Fig. 3, along with tables containing metrics for each baseline and for individual drivers, similar to Table I.

ACKNOWLEDGMENT

This project has received funding from the Flemish Agency for Innovation and Entrepreneurship (VLAIO) under Baekeland Mandaat No. HBC.2020.2263 (MIMIC) and research project No. HBC.2021.0939 (BECAREFUL) and has been supported by the European Union's Horizon 2020 research and innovation program under the grant agreement No. 953348 (ELO-X). Moreover, we would like to extend our gratitude to Vincent Van Ermengem and all the voluntary drivers for supporting the data collection.

REFERENCES

- [1] R. Reiter, J. Hoffmann, J. Boedecker, and M. Diehl, "A Hierarchical Approach for Strategic Motion Planning in Autonomous Racing," in *2023 European Control Conference (ECC)*, Jun. 2023, pp. 1–8.
- [2] B. Tearle, K. P. Wabersich, A. Carron, and M. N. Zeilinger, "A Predictive Safety Filter for Learning-Based Racing Control," *IEEE Robotics and Automation Letters*, vol. 6, no. 4, pp. 7635–7642, Oct. 2021, conference Name: IEEE Robotics and Automation Letters.
- [3] D. Kalaria, Q. Lin, and J. M. Dolan, "Towards Safety Assured End-to-End Vision-Based Control for Autonomous Racing," *IFAC-PapersOnLine*, vol. 56, no. 2, pp. 2767–2773, Jan. 2023. [Online]. Available: <https://www.sciencedirect.com/science/article/pii/S2405896323017810>
- [4] B. Amos, I. D. J. Rodriguez, J. Sacks, B. Boots, and J. Z. Kolter, "Differentiable MPC for End-to-end Planning and Control," Oct. 2019, arXiv:1810.13400 [cs, math, stat]. [Online]. Available: <http://arxiv.org/abs/1810.13400>
- [5] X. Xiao, T. Zhang, K. M. Choromanski, T.-W. E. Lee, A. Francis, J. Varley, S. Tu, S. Singh, P. Xu, F. Xia, S. M. Persson, D. Kalashnikov, L. Takayama, R. Frostig, J. Tan, C. Parada, and V. Sindhwani, "Learning Model Predictive Controllers with Real-Time Attention for Real-World Navigation," in *Proceedings of The 6th Conference on Robot Learning*. PMLR, Mar. 2023, pp. 1708–1721, iSSN: 2640-3498. [Online]. Available: <https://proceedings.mlr.press/v205/xiao23a.html>
- [6] F. S. Acerbo, J. Swevers, T. Tuytelaars, and T. D. Son, "Evaluation of MPC-based Imitation Learning for Human-like Autonomous Driving," *IFAC-PapersOnLine*, vol. 56, no. 2, pp. 4871–4876, Jan. 2023. [Online]. Available: <https://www.sciencedirect.com/science/article/pii/S2405896323016610>
- [7] "Chapter 3: Sensitivity Analysis under Second-Order Assumptions," in *Mathematics in Science and Engineering*. Elsevier, 1983, vol. 165, pp. 67–90. [Online]. Available: <https://linkinghub.elsevier.com/retrieve/pii/S0076539208606529>
- [8] J. A. E. Andersson, J. Gillis, G. Horn, J. B. Rawlings, and M. Diehl, "CasADi: a software framework for nonlinear optimization and optimal control," *Mathematical Programming Computation*, vol. 11, no. 1, pp. 1–36, Mar. 2019. [Online]. Available: <https://doi.org/10.1007/s12532-018-0139-4>
- [9] J. A. E. Andersson and J. B. Rawlings, "Sensitivity Analysis for Nonlinear Programming in CasADi," *IFAC-PapersOnLine*, vol. 51, no. 20, pp. 331–336, Jan. 2018. [Online]. Available: <https://www.sciencedirect.com/science/article/pii/S2405896318327137>
- [10] F. S. Acerbo, M. Alirzaei, H. Van Der Auweraer, and T. D. Son, "Safe Imitation Learning on Real-Life Highway Data for Human-like Autonomous Driving," in *2021 IEEE International Intelligent Transportation Systems Conference (ITSC)*, Sep. 2021, pp. 3903–3908. [Online]. Available: <https://ieeexplore.ieee.org/abstract/document/9564785>

- [11] “MOOG Motion Systems.” [Online]. Available: <https://www.moog.com/products/motion-systems.html>
- [12] “Simcenter Prescan.” [Online]. Available: <https://plm.sw.siemens.com/en-US/simcenter/autonomous-vehicle-solutions/prescan/>
- [13] “Simcenter Amesim.” [Online]. Available: <https://plm.sw.siemens.com/en-US/simcenter/systems-simulation/amesim/>
- [14] J. Debille, “SimRod experience: the electric vehicle digital twin demonstrator.” [Online]. Available: <https://blogs.sw.siemens.com/simcenter/the-simrod-experience-the-electric-vehicle-digital-twin-demonstrator/>
- [15] J. P. Allamaa, P. Listov, H. Van Der Auweraer, C. Jones, and T. D. Son, “Real-time Nonlinear MPC Strategy with Full Vehicle Validation for Autonomous Driving,” in *2022 American Control Conference (ACC)*, Jun. 2022, pp. 1982–1987, iSSN: 2378-5861. [Online]. Available: <https://ieeexplore.ieee.org/abstract/document/9867514>
- [16] M. Bojarski, D. Del Testa, D. Dworakowski, B. Firner, B. Flepp, P. Goyal, L. D. Jackel, M. Monfort, U. Muller, J. Zhang, X. Zhang, J. Zhao, and K. Zieba, “End to End Learning for Self-Driving Cars,” Apr. 2016, arXiv:1604.07316 [cs]. [Online]. Available: <http://arxiv.org/abs/1604.07316>

Learning from Visual Demonstrations through Differentiable Nonlinear MPC for Personalized Autonomous Driving: Supplementary Material

Flavia Sofia Acerbo^{1,2,3}, Jan Swevers^{2,4}, Tinne Tuytelaars³ and Tong Duy Son¹

APPENDIX

In the following sections, we provide supplementary material that we omitted due to space limitations in the main text of the paper "Learning from Visual Demonstrations through Differentiable Nonlinear MPC for Personalized Autonomous Driving," submitted to IROS 2024. This additional material comprises extra plots and metrics aimed at validating DriViDOC models, thereby enhancing the transparency of the study. Firstly, we present the complete set of trained DriViDOC models tested in closed-loop simulations. Secondly, we offer more detailed benchmarking results, including individual driver outcomes for the baselines and the results of statistical tests.

A. Closed-loop Testing

a) State Simulations: In Figures 1, 2, 3, 4, 5, 6 we show relevant states from closed-loop simulations of DriViDOC models, compared with the corresponding driver distribution. Figure 1 is equivalent to the one shown in Figure 3 from the main text. In each plot, we display pairs of models trained on different drivers, except for Figure 6, which exclusively showcases Model12. On the right axis, we indicate the curvature with a dashed line. In the d plots, the lane boundaries are shown as horizontal solid lines.

b) NMPC Parameters: Alongside the state simulations, we also provide the behavior of the NMPC dynamic parameters during the same closed-loop trajectories. These are illustrated in Figures 8, 9, 10, 12, and 11, corresponding to the same models depicted in the state simulation figures. Figure 7 mirrors Figure 4 in the main text. These plots offer valuable insights into how the different driving styles are realized by DriViDOC. The offsets \bar{d} and \bar{v}_x are normalized between -1 and 1. On the right axis, we indicate the curvature with a dashed line.

B. Benchmarking

a) Individual drivers results: In the main text, we present benchmarking results with baseline metrics averaged for all drivers in Table II. Here, we provide detailed results for each individual driver, similar to what we provided for DriViDOC in Table I of the main text. For the TRACK baseline, refer to Table I. For SF, refer to Table II. For NOIMG, refer to Table III.

b) Statistical Analysis: We present additional statistical results related to the benchmarking tests. In Figure 13 we show in the form of box-plots the mean Z-scores (MZ) of the relevant states for the TRACK, SF and NOIMG baseline, compared to DriViDOC. As mentioned in the main text, for NOIMG we exclude the models 00, 01, 08 and 09 due to convergence issues. In Figure 14, we show the same kind of representation for the MAE metrics.

Additionally, we assess the statistical significance of our results by conducting one-tailed paired-sample t-tests for each baseline. Specifically, we evaluate whether the baselines yield a statistically significant increase in the MZ and MAE metrics for each state compared to DriViDOC. In Table IV, the statistical results for TRACK are presented. DriViDOC demonstrates statistical superiority for v_x , a_x , and a_y , with notably low p-values, particularly for a_x , corroborating the qualitative findings outlined in the main text. However, the t-test for d is inconclusive, as no statistical significance of increase or decrease can be found. In Table V, the results for SF are presented. In this instance, DriViDOC exhibits superiority over SF for d , v_x , and a_y . However, the t-test for a_x is inconclusive, as no statistical significance of superiority or inferiority can be determined, which is not surprising as we highlighted in the main text that SF showed improvements in a_x for certain models. In Table VI, the results for NOIMG are presented. In this test, data from models 00, 01, 08, and 09 are excluded for both DriViDOC and NOIMG. Again, DriViDOC demonstrates statistical superiority for v_x , a_x , and a_y . The t-test on d is inconclusive as no statistical significance of superiority or inferiority can be found, even though, in Table II of the main text, it was shown that NOIMG was slightly better on average compared to DriViDOC.

¹Siemens Digital Industries Software, Leuven, Belgium

²Dept. of Mechanical Engineering, KU Leuven, Belgium

³Dept. of Electrical Engineering (ESAT), KU Leuven, Belgium

⁴Flanders Make@KU Leuven, Leuven, Belgium

Corresponding author email: flavia.acerbo@siemens.com

TABLE I: TRACK Baseline: performance metrics of the driving models for each driver. Less optimal results (Mean Z-score > 2) are highlighted with a red colour.

	d		v_x		a_x		a_y	
	AE [m]	Z-score	AE [m/s]	Z-score	AE [m/s ²]	Z-score	AE [m/s ²]	Z-score
Model00	0.20 ± 0.15	0.96 ± 0.84	0.78 ± 0.40	1.53 ± 0.81	0.20 ± 0.18	4.60 ± 4.38	0.38 ± 0.29	1.29 ± 0.99
Model01	0.39 ± 0.30	1.07 ± 0.99	0.83 ± 0.61	0.95 ± 0.89	0.36 ± 0.28	1.36 ± 1.73	0.39 ± 0.32	0.94 ± 0.89
Model02	0.18 ± 0.14	1.19 ± 0.99	2.05 ± 1.18	1.01 ± 0.66	0.43 ± 0.31	1.76 ± 1.41	0.67 ± 0.55	1.52 ± 1.25
Model03	0.52 ± 0.37	2.32 ± 2.59	0.67 ± 0.55	0.62 ± 0.55	0.40 ± 0.37	3.53 ± 6.59	0.52 ± 0.36	1.36 ± 1.34
Model04	0.41 ± 0.38	1.58 ± 1.67	1.69 ± 0.89	1.88 ± 1.22	0.76 ± 0.60	3.42 ± 2.94	0.61 ± 0.55	1.75 ± 2.16
Model05	0.23 ± 0.18	1.36 ± 1.41	1.03 ± 0.91	1.13 ± 1.03	0.35 ± 0.28	1.13 ± 1.29	0.27 ± 0.23	1.03 ± 0.91
Model06	0.38 ± 0.29	0.94 ± 0.76	1.93 ± 1.25	1.03 ± 0.83	0.38 ± 0.29	1.68 ± 1.71	0.39 ± 0.32	0.96 ± 0.99
Model07	0.49 ± 0.28	2.03 ± 1.47	1.51 ± 1.10	1.09 ± 0.89	0.49 ± 0.39	3.40 ± 5.08	0.36 ± 0.29	0.92 ± 0.82
Model08	0.40 ± 0.30	0.96 ± 0.76	1.31 ± 0.94	1.20 ± 0.95	0.46 ± 0.39	2.01 ± 2.47	0.84 ± 0.65	1.91 ± 1.73
Model09	0.67 ± 0.50	2.29 ± 2.36	1.05 ± 0.69	2.11 ± 1.83	0.46 ± 0.32	3.97 ± 4.27	0.56 ± 0.47	1.94 ± 2.02
Model10	0.31 ± 0.20	1.74 ± 1.56	1.40 ± 1.00	1.17 ± 1.17	0.65 ± 0.40	3.04 ± 3.84	0.54 ± 0.49	1.25 ± 1.49

TABLE II: SF Baseline: performance metrics of the driving models for each driver. Less optimal results (Mean Z-score > 2) are highlighted with a red colour.

	d		v_x		a_x		a_y	
	AE [m]	Z-score	AE [m/s]	Z-score	AE [m/s ²]	Z-score	AE [m/s ²]	Z-score
Model00	0.35 ± 0.22	1.73 ± 1.58	0.55 ± 0.36	1.18 ± 0.72	0.04 ± 0.11	0.75 ± 0.71	0.28 ± 0.22	0.99 ± 0.89
Model01	0.59 ± 0.40	1.71 ± 1.68	2.38 ± 2.02	2.91 ± 3.12	0.34 ± 0.27	0.95 ± 0.94	0.72 ± 0.61	1.64 ± 1.61
Model02	0.46 ± 0.33	3.18 ± 2.77	1.17 ± 0.74	0.55 ± 0.31	0.18 ± 0.15	0.71 ± 0.69	0.33 ± 0.26	0.83 ± 1.00
Model03	0.73 ± 0.54	3.14 ± 3.12	1.16 ± 0.89	1.12 ± 0.90	0.29 ± 0.29	2.65 ± 6.66	0.64 ± 0.82	1.45 ± 1.80
Model04	0.44 ± 0.29	1.85 ± 1.45	1.24 ± 1.08	1.28 ± 1.10	0.45 ± 0.49	1.26 ± 1.35	0.51 ± 0.46	1.35 ± 1.25
Model05	0.61 ± 0.37	3.76 ± 3.92	4.26 ± 1.63	3.90 ± 2.05	0.27 ± 0.22	0.78 ± 0.76	0.74 ± 0.53	2.40 ± 1.60
Model06	0.64 ± 0.41	2.11 ± 1.86	4.48 ± 2.48	2.21 ± 1.34	0.25 ± 0.21	1.02 ± 1.04	0.76 ± 0.61	1.50 ± 1.10
Model07	0.55 ± 0.41	2.28 ± 1.97	1.61 ± 1.17	1.17 ± 0.94	0.22 ± 0.21	0.86 ± 0.87	0.46 ± 0.37	1.08 ± 0.94
Model08	0.86 ± 0.53	2.06 ± 1.41	6.85 ± 3.66	7.15 ± 4.91	0.34 ± 0.28	2.63 ± 5.84	1.63 ± 1.08	3.54 ± 2.52
Model09	0.53 ± 0.37	1.87 ± 1.79	0.54 ± 0.34	1.04 ± 0.90	0.09 ± 0.13	0.54 ± 0.46	0.30 ± 0.25	0.95 ± 0.82
Model10	0.71 ± 0.54	3.93 ± 3.67	4.55 ± 2.49	3.44 ± 2.08	0.29 ± 0.23	1.07 ± 1.04	0.96 ± 0.67	1.90 ± 1.20

TABLE III: NOIMG Baselines: performance metrics of the driving models for each driver. Less optimal results (Mean Z-score > 2) are highlighted with a red color. The rows with a grey background correspond to the drivers with convergence to a high BC loss, who are excluded from average computations.

	d		v_x		a_x		a_y	
	AE [m]	Z-score	AE [m/s]	Z-score	AE [m/s ²]	Z-score	AE [m/s ²]	Z-score
Model00	1.60 ± 0.39	7.91 ± 4.20	13.67 ± 2.30	30.38 ± 9.85	0.14 ± 0.21	2.69 ± 1.88	2.55 ± 1.67	8.97 ± 7.38
Model01	1.75 ± 0.58	4.71 ± 2.95	12.21 ± 2.26	14.36 ± 7.50	0.34 ± 0.26	1.49 ± 2.47	2.16 ± 1.32	4.62 ± 3.37
Model02	0.15 ± 0.13	1.04 ± 1.01	4.11 ± 0.70	2.04 ± 0.74	0.24 ± 0.16	1.03 ± 0.74	1.00 ± 0.70	1.96 ± 1.27
Model03	0.31 ± 0.25	1.34 ± 1.44	1.73 ± 0.97	1.65 ± 0.97	0.43 ± 0.31	5.26 ± 9.36	0.62 ± 0.47	1.35 ± 0.95
Model04	0.24 ± 0.23	0.93 ± 0.87	1.49 ± 1.38	1.61 ± 1.57	0.57 ± 0.48	2.33 ± 2.19	0.63 ± 0.48	1.64 ± 1.23
Model05	0.52 ± 0.37	3.01 ± 2.80	2.09 ± 1.42	1.86 ± 1.64	0.29 ± 0.23	0.81 ± 0.68	0.35 ± 0.27	1.30 ± 1.09
Model06	0.28 ± 0.27	0.90 ± 1.11	3.27 ± 2.11	1.73 ± 1.42	0.23 ± 0.17	1.00 ± 1.03	0.68 ± 0.67	1.53 ± 1.68
Model07	0.31 ± 0.29	1.31 ± 1.28	3.15 ± 1.62	2.30 ± 1.33	0.33 ± 0.25	2.00 ± 2.62	0.65 ± 0.51	1.50 ± 1.16
Model08	1.48 ± 0.54	3.55 ± 1.95	13.65 ± 2.62	14.14 ± 6.51	0.43 ± 0.25	2.98 ± 3.40	2.56 ± 1.40	5.23 ± 3.46
Model09	1.57 ± 0.58	5.41 ± 4.07	12.53 ± 2.18	24.69 ± 14.27	0.17 ± 0.19	1.43 ± 1.53	2.32 ± 1.40	7.88 ± 6.42
Model10	0.22 ± 0.15	1.30 ± 1.13	1.88 ± 1.24	1.50 ± 1.25	0.43 ± 0.32	1.94 ± 3.80	0.60 ± 0.51	1.30 ± 1.15

TABLE IV: Results of the one-tailed paired-sample t-test, validating increase on MAE and MZ for TRACK compared to DriViDOC. Statistically significant increases are highlighted in bold.

	d	v_x	a_x	a_y
MAE	p=0.514, stat=-0.04	p=0.017, stat=2.45	p=0.000, stat=7.10	p=0.011, stat=2.70
MZ	p=0.618, stat=-0.31	p=0.026, stat=2.21	p=0.000, stat=5.43	p=0.015, stat=2.54

TABLE V: Results of the one-tailed paired-sample t-test, validating increase on MAE and MZ for SF compared to DriViDOC. Statistically significant increases are highlighted in bold.

	d	v_x	a_x	a_y
MAE	p=0.001, stat=3.97	p=0.012, stat=2.65	p=0.158, stat=1.05	p=0.018, stat=2.43
MZ	p=0.002, stat=3.65	p=0.017, stat=2.46	p=0.464, stat=0.09	p=0.023, stat=2.28

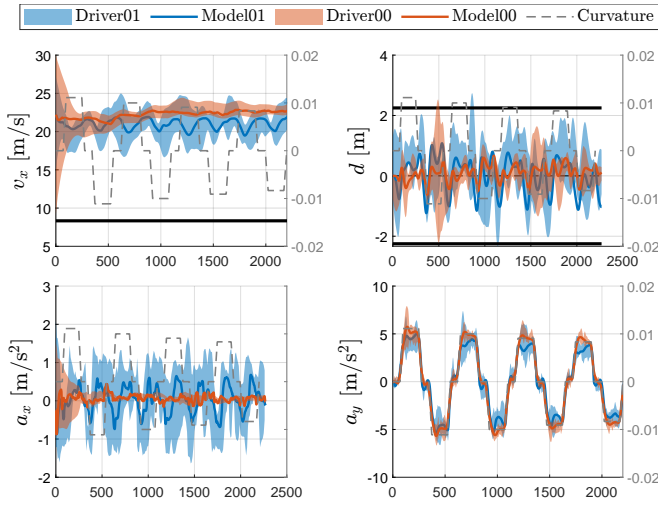


Fig. 1: DriViDOC models 00 and 01, compared with the corresponding driver distribution.

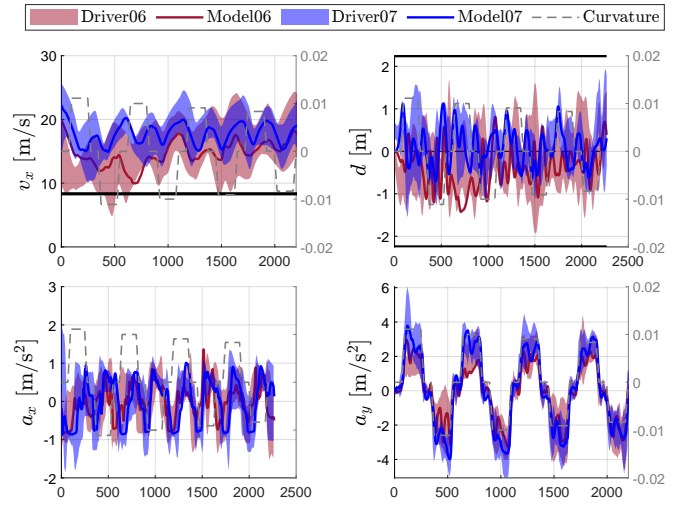


Fig. 4: DriViDOC models 06 and 07, compared with the corresponding driver distribution.

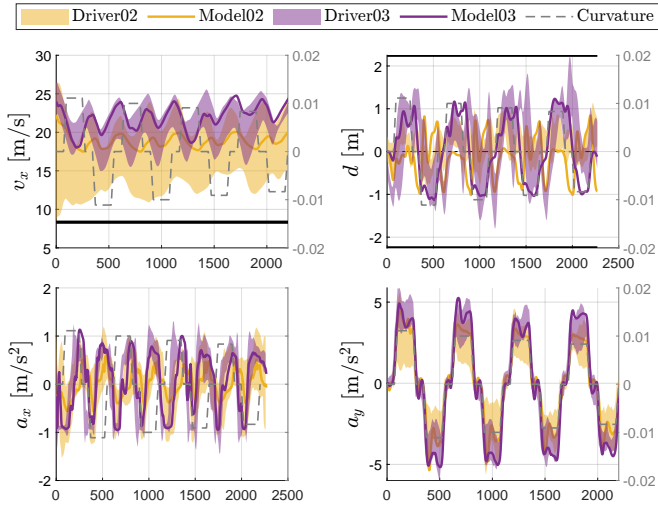


Fig. 2: DriViDOC models 02 and 03, compared with the corresponding driver distribution.

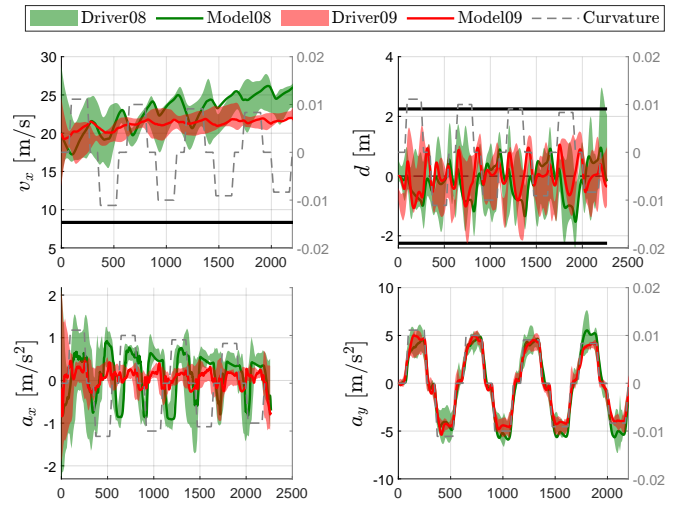


Fig. 5: DriViDOC models 08 and 09, compared with the corresponding driver distribution.

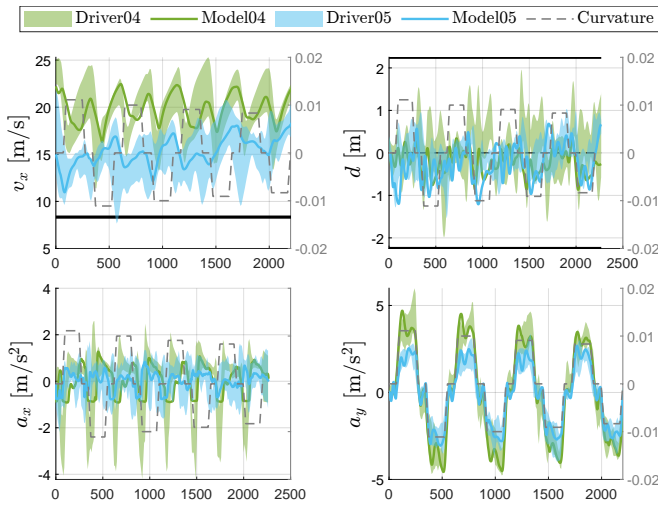


Fig. 3: DriViDOC models 04 and 05, compared with the corresponding driver distribution.

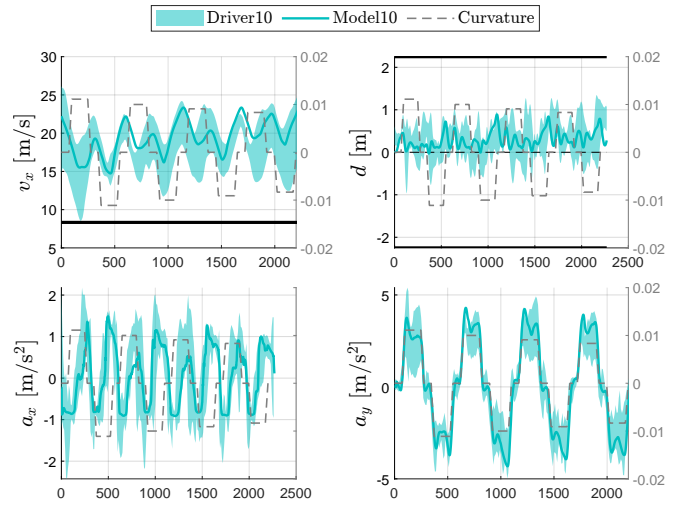


Fig. 6: DriViDOC model 12, compared with the corresponding driver distribution.

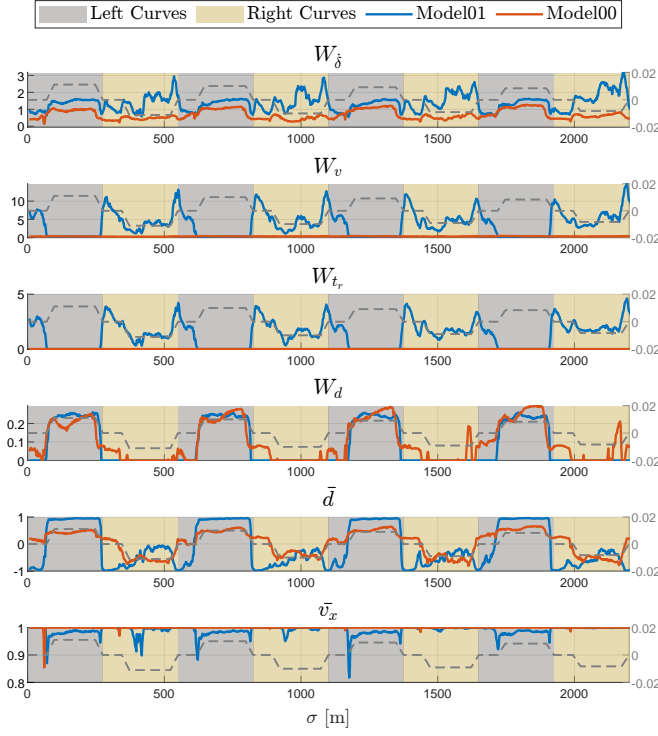


Fig. 7: Parameters $\mathbf{p}(t)$ values from closed-loop simulations of DriViDOC models 00 and 01.

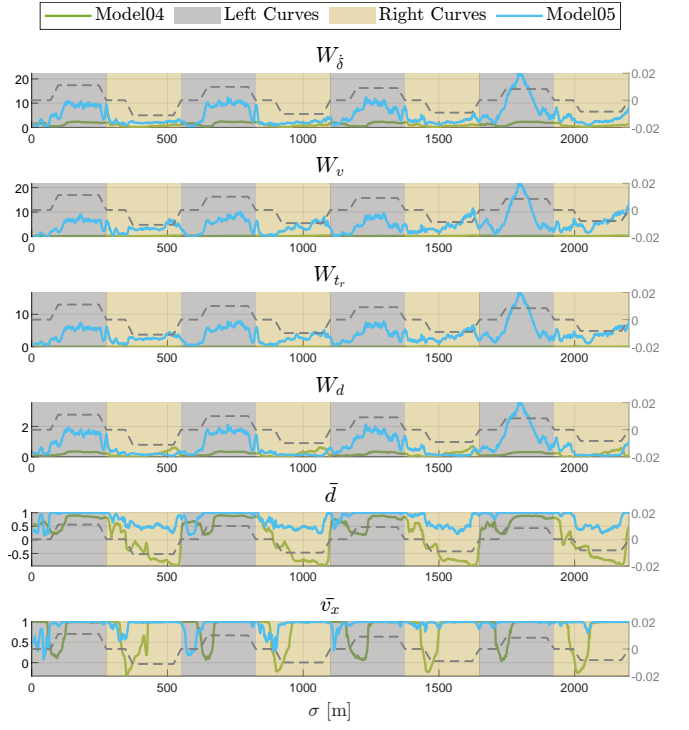


Fig. 9: Parameters $\mathbf{p}(t)$ values from closed-loop simulations of DriViDOC models 04 and 05.

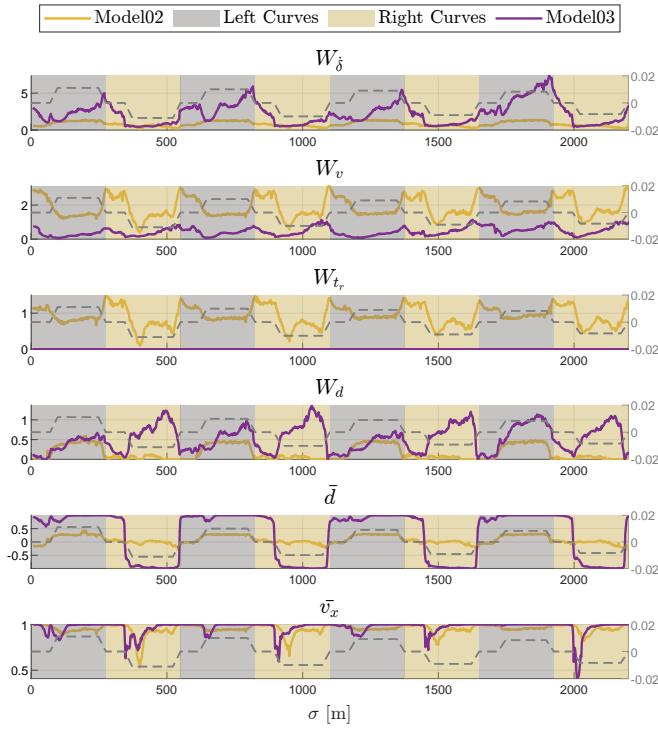


Fig. 8: Parameters $\mathbf{p}(t)$ values from closed-loop simulations of DriViDOC models 02 and 03.

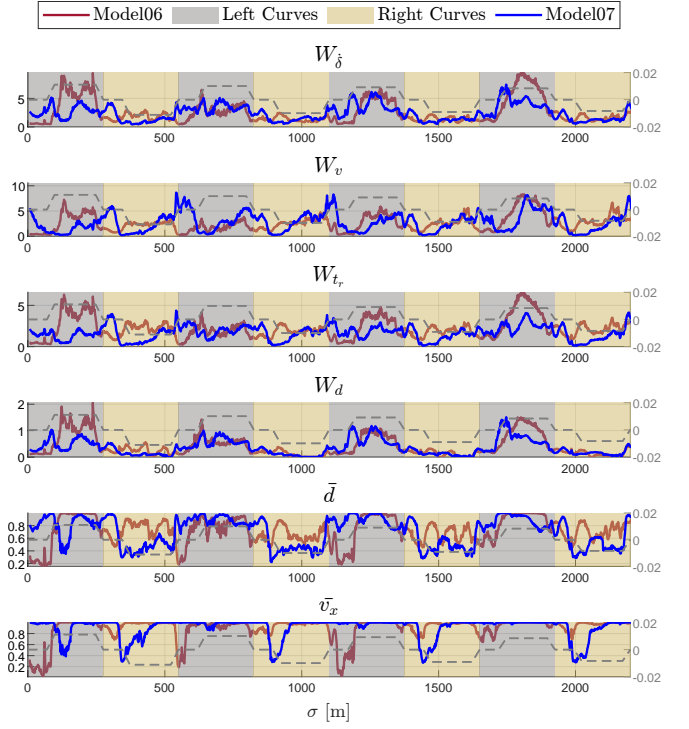


Fig. 10: Parameters $\mathbf{p}(t)$ values from closed-loop simulations of DriViDOC models 06 and 07.

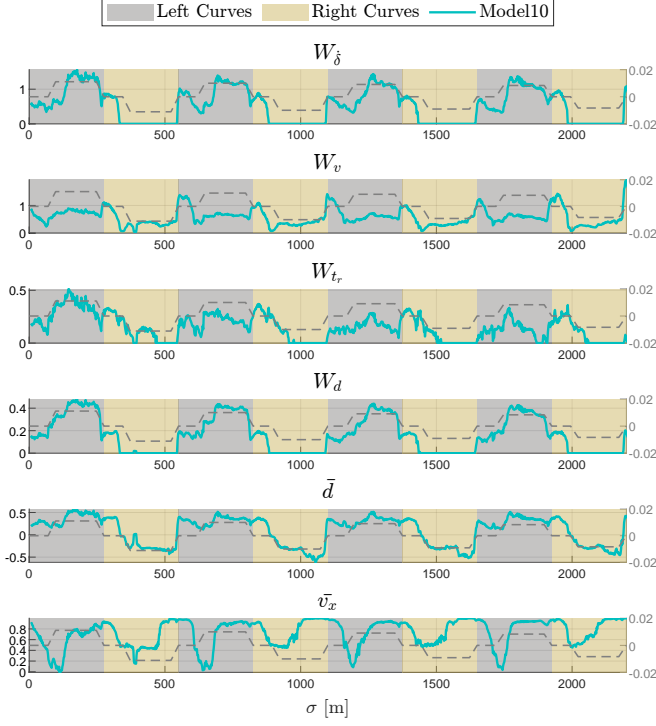


Fig. 11: Parameters $\mathbf{p}(t)$ values from closed-loop simulations of DriViDOC model 12.

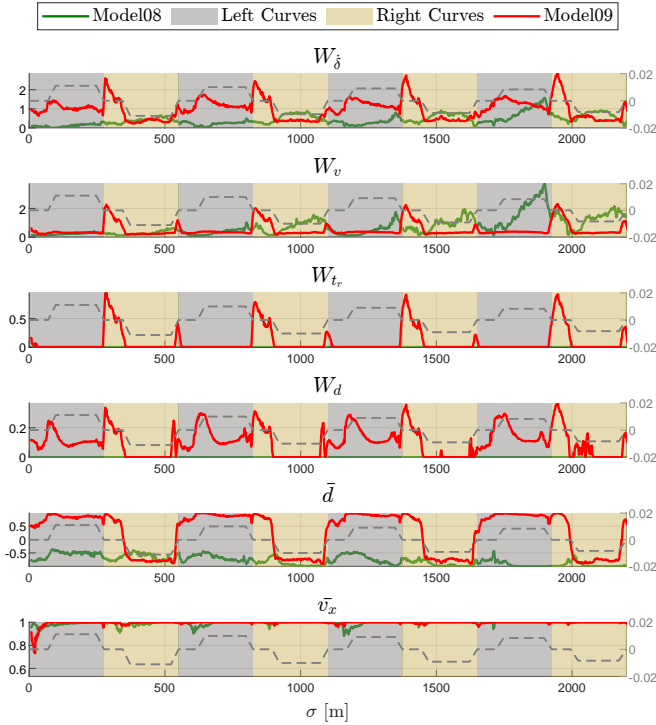


Fig. 12: Parameters $\mathbf{p}(t)$ values from closed-loop simulations of DriViDOC models 08 and 09.

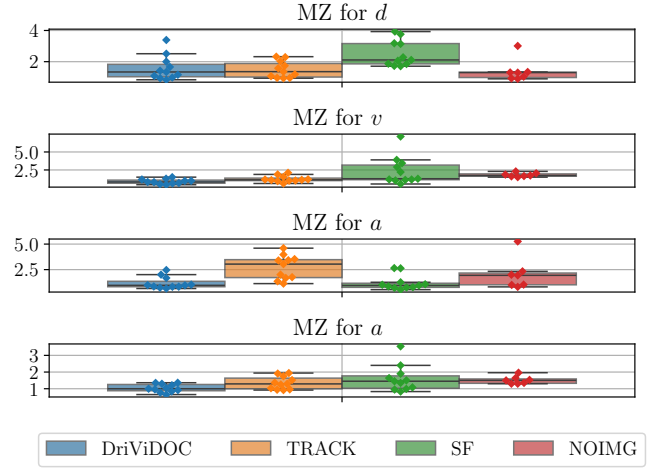


Fig. 13: DriViDOC benchmarking against TRACK, SF and NOIMG baselines. Box plots of the Mean Z-score (MZ), computed with respect to the driver's distributions, for states d , v_x , a_x and a_y .

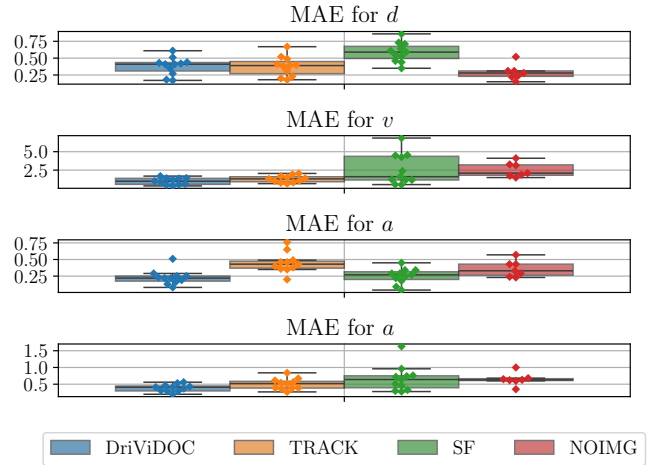


Fig. 14: DriViDOC benchmarking against TRACK, SF and NOIMG baselines. Box plots of the Mean Absolute Error (MAE), computed with respect to the driver's distributions, for states d , v_x , a_x and a_y .

TABLE VI: Results of the one-tailed paired-sample t-test, validating increase on MAE and MZ for NOIMG compared to DriViDOC. Models trained on drivers 00,03,10 and 11 have been excluded from the test (see main text). Statistically significant increases are highlighted in bold.

	d	v_x	a_x	a_y
MAE	$p=0.897$, stat=-1.42	$p=0.006$, stat=3.53	$p=0.011$, stat=3.07	$p=0.004$, stat=3.89
MZ	$p=0.837$, stat=-1.07	$p=0.005$, stat=3.64	$p=0.037$, stat=2.15	$p=0.007$, stat=3.48